Original Article

MOLECULAR METABOLISM

Maternal high-fat diet exaggerates diet-induced insulin resistance in adult offspring by enhancing inflammasome activation through noncanonical pathway of caspase-11

Naotoshi Wada [1], Hiroyuki Yamada [1,*], Shinichiro Motoyama [1], Makoto Saburi [1], Takeshi Sugimoto [1], Hiroshi Kubota [1], Daisuke Miyawaki [1], Noriyuki Wakana [1], Daisuke Kami [2], Takehiro Ogata [3], Satoaki Matoba [1]

ABSTRACT

Objective: Maternal high-fat diet (HFD) has been shown to promote the development of insulin resistance (IR) in adult offspring; however, the underlying mechanisms remain unclear.

Methods: Eight-week-old female wild-type mice (C57BL/6) were fed either an HFD or a normal diet (ND), one week prior to mating, and the diet was continued throughout gestation and lactation. Eight-week-old male offspring of both groups were fed an HFD for 8 weeks.

Results: Offspring of HFD-fed dams (O-HFD) exhibited significantly impaired insulin sensitivity compared with the offspring of ND-fed dams (O-ND). The adipocyte size of the eWAT increased significantly in O-HFD and was accompanied by abundant crown-like structures (CLSs), as well as a higher concentration of interleukin 1β (IL-1β) in the eWAT. Treatment with an inflammasome inhibitor, MCC950, completely abrogated the enhanced IR in O-HFD. However, ex vivo caspase-1 activity in eWAT revealed no difference between the two groups. In contrast, noncanonical inflammasome activation of caspase-11 was significantly augmented in O-HFD compared with O-ND, suggesting that membrane pore formation, but not cleavage of pro-IL-1β by caspase-1, is augmented in O-HFD. To examine the membrane pore formation, we performed metabolic activation of bone marrow-derived macrophages (BMDMs). The percentage of pore formation assessed by ethidium bromide staining was significantly higher in BMDMs of O-HFD, accompanied by an enhanced active caspase-11 expression. Consistently, the concentration of IL-1β in culture supernatants was significantly higher in the BMDMs from O-HFD than those from O-ND.

Conclusions: These findings demonstrate that maternal HFD exaggerates diet-induced IR in adult offspring by enhancing noncanonical caspase-11-mediated inflammasome activation.

Keywords Maternal high-fat diet; Insulin resistance; Inflammasome; Interleukin-1β; Caspase-1; Caspase-11

1. INTRODUCTION

Obesity is a worldwide epidemic [1,2] and intimately associated with the development of metabolic disorders and type 2 diabetes, leading to the development of cardiovascular diseases [3–5]. Despite extensive efforts, the prevalence of obesity and metabolic disorders has been strikingly increased; therefore, novel therapeutic approaches are currently needed [6]. Maternal nutrition throughout pregnancy and lactation has been well recognized to increase the offspring's risk of obesity and metabolic disorders across the life span [7–11]. Nutrient status during fetal development has been shown to modulate gene expressions in offspring adipose tissue without alterations in the DNA sequence, which is referred to as "epigenetic programing" [12–15]. However, the underlying mechanism by which developmental modifications of adipose tissue promote insulin resistance (IR) in offspring remains to be fully elucidated [16–19], and a potential therapeutic strategy has not yet been established.

We have shown that maternal high-fat diet (HFD) exaggerates atherosclerosis development in offspring through enhanced macrophage-mediated inflammatory response [20]. Given that HFD-induced IR is closely implicated with the augmented accumulation of macrophages [21–23] and subsequent inflammatory response in adipose tissue [24–26], it is likely that developmental modification of monocytes/macrophages plays a critical role in HFD-induced IR in offspring. Recently, a nucleotide-binding domain, leucine-rich repeat-containing family, pyrin domain-containing-3- (NLRP3-) dependent inflammasome activation has also been associated with the exaggeration of IR [27–30]. However, underlying mechanisms of maternal

[1]Department of Cardiovascular Medicine, Graduate School of Medical Science, Kyoto Prefectural University of Medicine, Kyoto, Japan [2]Department of Regenerative Medicine, Graduate School of Medical Science, Kyoto Prefectural University of Medicine, Kyoto, Japan [3]Department of Pathology and Cell Regulation, Graduate School of Medical Science, Kyoto Prefectural University of Medicine, Kyoto, Japan

*Corresponding author. Department of Cardiovascular Medicine, Graduate School of Medical Science, Kyoto Prefectural University of Medicine, 465 Kajii-cho, Kamigyo-ku, Kyoto 602-8566, Japan. Fax: +81 75 251 5514. E-mail: hiyamada@koto.kpu-m.ac.jp (H. Yamada).

Received February 8, 2020 • Revision received March 22, 2020 • Accepted March 31, 2020 • Available online 6 April 2020

https://doi.org/10.1016/j.molmet.2020.100988

HFD-induced inflammasome activation in the context of developmental reprograming of monocytes/macrophages and their relevant contribution to HFD-induced IR remained obscure.

Here, we examined phenotypic alterations in offspring macrophages by maternal HFD and investigated their roles in IR development. Maternal HFD exaggerated IR development in adult offspring, accompanied by enhanced IL-1β release in epididymal white adipose tissue (eWAT). Treatment with inflammasome inhibitor completely eliminated the exaggerated IR development in offspring of HFD-fed dams to an extent similar to that in the offspring of ND-fed dams. Moreover, augmented pore formation by enhanced noncanonical activation pathway of caspase-11, but not canonical activation pathway of caspase-1, may contribute to the significant release of IL-1β in bone-marrow-derived macrophages (BMDMs) of the offspring of HFD-fed dam. Our findings suggest that maternal HFD-induced reprograming of the offspring monocytes/macrophages contributes to IR development and that therapeutic targeting of the phenotypic changes of monocytes/macrophages could potentially remediate and prevent cardiovascular diseases in adult offspring.

2. MATERIALS AND METHODS

2.1. Experimental animals

All experiments were performed with strict adherence to "Directive 2010/63/EU" of the European Parliament and to the Guidelines for Animal Experiments of the Kyoto Prefectural University of Medicine, following approval by the Institutional Animal Care and Use Committee of the Kyoto Prefectural University of Medicine.

Wild-type mice (C57BL/6) were obtained from *Shimizu Laboratory Supplies Co., Ltd.* (Kyoto, Japan). Eight-week-old female mice were maintained on a normal diet (ND) (12.0% fat, 28.9% protein, and 59.1% carbohydrate; Oriental Yeast Co., Tokyo, Japan) or HFD (energy content: 62.2% fat, 18.2% protein, and 19.6% carbohydrate; Oriental Yeast Co.) one week before mating, as well as throughout pregnancy and lactation. All offspring were weaned at 5 weeks of age and fed an ND until the age of 8 weeks; they were then switched to an HFD until the age of 16 weeks, following which glucose tolerance and insulin sensitivity were evaluated. For NLRP3 inflammasome inhibitor, MCC950 (AdipoGen Life Sciences, San Diego, CA, USA) was intraperitoneally administered three times every week (10 mg/kg) during the 8 weeks of HFD feeding, as previously described [31]. For the bone marrow transplantation (BMT) experiment, eight-week-old male recipient offspring of HFD-fed dam (O-HFD) were lethally irradiated with 9 Gy using an X-ray source (SOFTEX CO., Ltd. Tokyo, Japan) [32]. Bone marrow (BM) cells were harvested from the femurs and tibias of eight-week-old donor male offspring of O-ND-fed dam (O-ND) or O-HFD by flushing with RPMI-1640 medium (Thermo Fisher Scientific, Waltham, MA, USA), and recipients received 5×10^6 BM cells per mouse in 0.2 mL of the medium by tail vein injection. Five weeks after BMT, all mice were then switched to an HFD until the age of 25 weeks, following which glucose tolerance and insulin sensitivity were evaluated.

Animals were housed in a room maintained at 22 °C under a 12-hour light/dark cycle and provided with drinking water *ad libitum*. After 8 weeks of HFD feeding, mice were euthanized by transcardial perfusion under anesthesia induced by isoflurane (2%; 0.2 mL/min).

2.2. Experimental procedures

2.2.1. Assessment of body weight and food intake

Body weight was measured biweekly after starting HFD feeding. The average food intake per cage was monitored during HFD feeding, including spillage, by measuring the weight of food pellets (g) in cages with five similarly aged mice.

2.2.2. Glucose and insulin tolerance test

GTT was performed on 16-week-old mice after an overnight fast. Blood glucose concentrations were measured at 0 min before and 15, 30, 60, 90, and 120 min after intraperitoneal injection of glucose (2 g/kg body weight). For insulin tolerance test (ITT), insulin (1 U/kg body weight in 0.1% distilled water; Humulin R-Insulin, Eli Lilly Japan K.K. Kobe, Japan) was intraperitoneally injected after an overnight fast. Blood glucose concentrations were measured 0 min before and 30, 60, 90, and 120 min after injection.

2.2.3. Serum lipids analysis

Measurements of triglyceride, free fatty acid (FFA), and total cholesterol were outsourced to SRL, Tokyo, Japan.

2.2.4. Enzyme-linked immunosorbent assay (ELISA)

Blood was collected into tubes from the left ventricle. The serum was separated by centrifugation at $2{,}000 \times g$ for 20 min and stored at −80 °C. The concentrations of insulin, IL-1β, and TNF-α in serum, eWAT, and culture supernatant were estimated using an ELISA Kit (Mouse insulin ELISA KIT, MS303, Morinaga Institute of Biological Science, Yokohama, Japan; Mouse IL-1 beta/IL-1F2 Quantikine ELISA Kit, MLB00C, R&D Systems, Minneapolis, MN, USA; Mouse TNF-alpha Quantikine ELISA Kit, MTA00B, R&D Systems) according to the manufacturer's instructions.

2.2.5. Quantitative real-time polymerase chain reaction (qPCR)

Total RNA was extracted from adipose tissue using the RNeasy Lipid Tissue Mini Kit (74804; Qiagen, Hilden, Germany) and reverse transcribed to prepare cDNA using the TAKARA PrimeScript RT Reagent Kit with gDNA Eraser (RR047A; Takara Bio, Shiga, Japan). Real-time PCR was performed using a Thermal Cycler Dice System (Takara Bio), with the KAPA SYBR® FAST Universal qPCR Kit (KK4602; KAPA Biosystems, Wilmington, MA, USA). Dissociation curves were examined for the aberrant formation of primer dimers. The threshold cycle (CT) values were normalized to GAPDH, and the relative expression was calculated by the ΔΔCT method. Data were expressed as gene expression levels relative to those of controls. The following primer pairs were used (Supplementary Table).

2.2.6. Flow cytometry

BM promonocytes and peripheral blood monocytes were identified using FACS analysis. For staining BM promonocytes, antibodies against anti-mouse APC-conjugated CD11b (clone M1/70; BD Biosciences, San Jose, CA, USA) and FITC-conjugated Ly-6G (clone 1A8; BD Biosciences) were used [32]. For staining of peripheral monocytes, anti-mouse FITC-conjugated B220 (clone RA3-6B2; BD Biosciences), CD11c (clone HL; BD Biosciences), NK1.1 (clone PK136; BD Biosciences), CD49b (clone DX-5; BD Biosciences), CD90.2 (clone 53-2.1; BD Biosciences), Ly-6G (clone 1A8; BD Biosciences), F4/80 (clone BM8; BioLegend, San Diego, CA, USA), and I-Ab (clone 25-9-17, BioLegend) antibodies were used as lineage markers. Blood cells were stained with APC-conjugated CD11b (clone M1/70; BD Biosciences) and APC-Cy7-conjugated Ly-6C (clone HK1.4; Biolegend) antibodies, as previously described [33]. For epididymal white adipose tissue (eWAT) macrophages, stromal vascular cells were stained with PerCP-Cy5.5-conjugated anti-CD45 (clone 30-F11; BD Biosciences), PE-conjugated anti-F4/80 (clone BM8; eBioscience, Wien, Austria), FITC-conjugated anti-CD11b (clone M1/70; BD Biosciences), PE-Cy7-conjugated anti-CD11c (clone N418;

eBioscience), and APC-conjugated anti-CD206 (clone C068C2; BioLegend) antibodies, which identify discrete M1-like and M2-like adipose tissue macrophage subsets in obese mice [34]. For caspase-1 activity, cells were cultured and stimulated as stated below [35]. Green FLICA Caspase-1 Assay Kit (FAM-FLICA® Caspase-1 Assay Kit; ImmunoChemistry Technologies, LLC, Bloomington, MN, USA) was used according to the provided protocol. Cell counting was done with Sony SH800 (Sony Biotechnology Inc. Tokyo, Japan). Data were processed using FlowJo software (BD Biosciences).

2.2.7. Ex vivo caspase-1 activity

On experiment day, all animals were administered with 100 μL Red-YVAD-FMK (Vergent Bioscience Inc., Minneapolis, MN, USA), via tail vein injection. The Red-YVAD-FMK is targeted fluorescence imaging tracers comprised of a caspase recognition sequence, a fluoromethyl ketone (FMK) leaving group and a red fluorescent label. FMK-derivatized peptides act as effective irreversible inhibitors with no added cytotoxic effects. The probes will preferentially and irreversibly bind to active caspases, causing apoptotic cells to fluoresce. Three hours after injection, the liver and eWAT were harvested and then ex vivo liver and eWAT imaging was immediately performed using an *in vivo* imaging system (IVIS) Lumina Series III Optical Imaging Platform (PerkinElmer Inc. Waltham, MA, USA) using the red filter sets (excitation range, 660 nm; emission, 710 nm longpass filter). We manually drew regions of interest (ROI) encompassing the whole organs, and the resulting signal was computed in the units of scaled counts per second. We carefully ensured that the size of the ROIs drawn across animal samples was consistent.

2.2.8. *In vitro* activation of BMDMs

Primary cultures of BMDMs were obtained from femurs and tibias of 8-week-old mice and cultured in the complete medium (DMEM supplemented with 10% fetal bovine serum (FBS) and 1% penicillin/streptomycin, 1 ng/mL Macrophage-Colony Stimulating Factor-1 (15% L-929-conditioned medium)). Nonadherent cells were collected after 24 h and differentiated for seven days yielding 98% F4/80^{+} cells. For classical and alternative BMDM polarization assay, BMDMs were treated with either 100 U/mL IFN-γ (M1-like) or 100 ng/mL IL-4 (M2-like) [36]. For metabolic activation, differentiated bone-marrow-derived macrophages were polarized with 200 ng/mL lipopolysaccharide (LPS, Sigma—Aldrich, St. Louis, MO, USA) for 3 h and 400 μM palmitate (PA) (Sigma—Aldrich)-bovine serum albumin (BSA), 10 nM insulin, and 30 mM glucose for 3 h [27].

2.2.9. Western blotting

BMDMs and eWAT were harvested and homogenized in Eppendorf tubes in 100 μL of lysis buffer (50 mmol/L Tris—HCl (pH 7.5), 150 mmol/L NaCl, 50 mmol/L EDTA, 1% Triton X-100, and protease—phosphatase inhibitor mixture). Protein samples were subjected to SDS-PAGE and then transferred to membranes that were subsequently incubated with primary antibodies against GSDMD (STJ112203; St John's Laboratory, London, UK), caspase-11 (ab180673, EPR18628; Abcam, Cambridge, UK), caspase-1 (EPR16883, ab179515, Abcam), α-tubulin (T5168, B-5-1-2, Sigma—Aldrich, St. Louis, MO, USA), and β-actin (A2228, AC-74; Sigma—Aldrich). Immunoreactive proteins were visualized with an ECL-enhanced chemiluminescence detection system (GE Healthcare Life Sciences, Marlborough, MA, USA) followed by exposure to ChemiDoc XRS + imaging system (Bio-Rad Laboratories, Inc. Hercules, CA, USA). The bands were quantified by ImageJ v1.50i software (https://imagej.nih.gov/ij/index.html). α-tubulin or β-actin was as references.

2.2.10. LDH assay

BMDMs were primed with LPS for 3 h and subsequently treated with PA-BSA, insulin, and glucose for 3 h. Medium alone was used as the negative control, and 2% Triton X was used as positive control. Supernatants from controls and samples were reserved for the assay. Percent of LDH release was assayed using the LDH Cytotoxicity Detection Kit (MK401; Takara Bio). The assay was conducted as recommended. The absorbance was measured using Bio-Rad iMark (Bio-Rad Laboratories, Inc.) at 490 nm.

2.2.11. Pore formation assay

Pore formation was assayed by ethidium bromide (EtBr) (Invitrogen, Carlsbad, CA, USA) staining as described previously [37]. In this assay, 1×10^6 BMDMs were added on a 6-well plate. After LPS priming for 3 h, cells were untreated or treated with PA-BSA, insulin, and glucose containing 1:1000 Hoechst 33342 (AdipoGen Life Sciences) and 1:1000 EtBr. All cells were stained with Hoechst, whereas only cells with membrane pores allowed diffusion of EtBr into the cell. Pore formation activity was measured as the percentage of BMDMs that stained positive with EtBr. Images were acquired using JuLi™ Stage automated imaging system (NanoEntek Inc., Seoul, South Korea). Time-lapse images were captured every 30 min at 10X magnification.

2.3. Statistical analysis

We performed a Kolmogorov—Smirnov test for the normality of all continuous variables. A P value above 0.05 indicated that the data were normally distributed, and data were expressed as the mean ± standard error of the mean (SEM). Mean values were compared using analysis of variance (ANOVA) followed by a Tukey—Kramer test to analyze significant differences between the groups. A P value below 0.05 was considered statistically significant. Significant differences among groups for dependent variables were detected using two-way ANOVA: maternal diet (ND versus HFD) and LPS priming (before priming versus after priming). A P value below 0.05 was considered statistically significant.

3. RESULTS

3.1. Maternal HFD accelerates the development of HFD-induced IR in adult offspring

After 8 weeks of HFD feeding, the ITT showed significant impairment of insulin sensitivity in male O-HFD, whereas a glucose tolerance test did not show any difference between the two groups (Figure 1A,B). Consistently, serum insulin levels and homeostasis model assessment- (HOMA-) IR were significantly higher in O-HFD than those in O-ND (Figure 1C). The mean body weight (BW) and eWAT weight/BW were significantly increased after HFD feeding; however, there was no difference between the two groups (Supplementary Figure 1). Further, glucose tolerance and insulin sensitivity before HFD feeding and after 8 weeks of ND feeding were comparable between the two groups (Supplementary Figures 2A,B). These findings suggest that maternal-associated IR is independent of food intake and BW gain in offspring and is exhibited in HFD-fed offspring. Maternal-associated IR was also observed in HFD-fed female offspring (Supplementary Figure 3). To further examine the substantial role of BM cells to impaired insulin sensitivity in O-HFD, BMT experiment was performed. Glucose tolerance and insulin tolerance in O-HFD transplanted with BM cells from O-HFD were significantly impaired compared with those in O-HFD transplanted with BM cells from O-ND (Supplementary Figure 4), suggesting that BM cells substantially contribute to the exaggerated development of IR in O-HFD. Percentages of BM promonocytes were

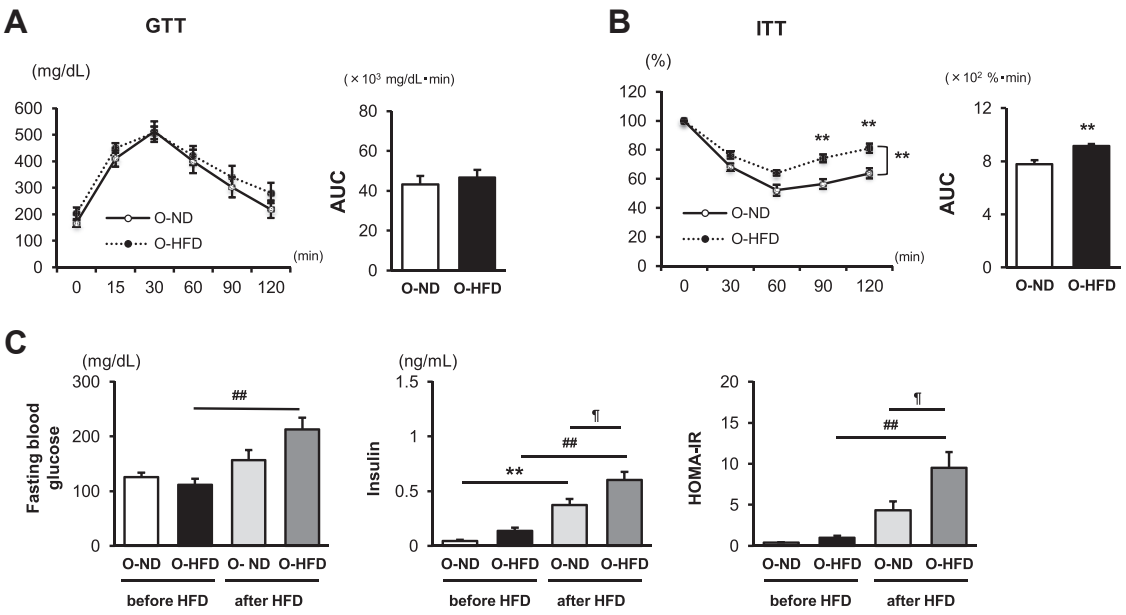

Figure 1: Maternal HFD accelerates the development of HFD-induced insulin resistance. (**A and B**) Glucose and insulin tolerance tests after 8 weeks of HFD. Values represent the mean ± SEM for 9 O-ND and 9–10 O-HFD mice. $^{**}P < 0.01$ versus O-ND. O-ND, offspring of ND-fed dam; O-HFD, offspring of HFD-fed dam; GTT, glucose tolerance test; ITT, insulin tolerance test; AUC, area under the curve. (**C**) Serum concentrations of fasting blood glucose and insulin, and homeostatic model assessment- (HOMA-) IR before and after 8 weeks of HFD. Values represent the mean ± SEM for 7 O-ND and 10 O-HFD mice before HFD, as well as 8 O-ND and 8 O-HFD mice after 8 weeks of HFD. $^{**}P < 0.01$ versus O-ND before HFD. $^{\#\#}P < 0.01$ versus O-HFD before HFD. $^{¶}P < 0.05$ versus O-ND after HFD. O-ND, offspring of ND-fed dam; O-HFD, offspring of HFD-fed dam.

comparable between the two groups before and after HFD feeding (Supplementary Figure 5). Likewise, the percentages of circulating inflammatory monocytes were equivalent between the two groups after HFD feeding (Supplementary Figure 6). These findings suggest that maternal HFD does not affect BM monocytosis and subsequent mobilization to the peripheral blood.

3.2. Maternal HFD augments proinflammatory response in eWAT

Epididymal adipose tissue weight was significantly increased after HFD feeding in both groups of mice (Supplementary Figure 1); however, the size of adipocyte and the number of crown-like structures (CLSs) were markedly increased in O-HFD compared with those in O-ND (Figure 2A–C). Consistently, mRNA expression levels of F4/80, MCP-1, and ICAM-1 were significantly higher in O-HFD than those in O-ND (Figure 2D). We next examined the fractions of eWAT macrophages by flow cytometric analysis. M1-like macrophage fraction in O-HFD was significantly increased while M2-like macrophage fraction was comparable between the two groups (Figure 2E,F). Further, eWAT concentration of IL-1β in O-HFD was markedly increased after HFD feeding and much higher than O-ND (Figure 2G), whereas eWAT concentration of TNF-α after HFD feeding was comparable between the two groups (Supplementary Figure 7). This finding tempts us to hypothesize that inflammasome activation is augmented in eWAT of O-HFD.

3.3. Inflammasome inhibitor treatment completely abolishes the augmented IR development in offspring of HFD-fed dam

To examine the involvement of inflammasome activation in exaggerated IR in O-HFD, NLRP3 inflammasome inhibitor, MCC950, was administered during HFD feeding. Treatment with MCC950 significantly attenuated HFD-induced increase in BW; however, there was no difference between the O-ND and O-HFD. In contrast, eWAT/BW ratio was not affected by MCC950 treatment in both O-ND and O-HFD (Supplementary Figure 8). MCC950-treated offspring showed a significant improvement in insulin tolerance, and no significant difference could be observed between the two groups (Figure 3A). Consistently, the adipocyte size and the number of CLSs were markedly decreased in MCC950-treated O-HFD compared with those in PBS-treated O-HFD, resulting in no apparent difference between the two groups of MCC950-treated offspring (Figure 3B,C). Likewise, IL-1β concentration in eWAT was significantly decreased in MCC950-treated O-HFD to a similar extent as O-ND (Figure 3D). These findings support the notion that augmented inflammasome activation in O-HFD substantially contributes to the augmented IR development in O-HFD.

3.4. Noncanonical inflammasome activation pathway of caspase-11 is enhanced in eWAT of offspring of HFD-fed dam

In the canonical inflammasome activation pathway, active caspase-1 cleaves gasdermin D (GSDMD) as well as pro-IL-1β to mature IL-1β [38]. An n-terminal portion of cleaved GSDMD moves to the cell membrane to make pore formation, which promotes the extravasation of mature IL-1β [39–42]. We, therefore, examined ex vivo caspase-1 activity in eWAT by a fluorescent image of IVIS. But unexpectedly, caspase-1 activity was equivalent between the two groups of eWAT (Figure 4A,B). We also examined the caspase-1 activation in the liver and serum level of FFA; however, there was no difference between the two groups (Supplementary Figure 9A,B). We next examined the noncanonical inflammasome activation pathway of caspase-11, which has been shown to cleave GSDMD, but not pro-IL-1β, and promote membrane pore formation [43–45]. We observed a trend toward a higher expression level of cleaved GSDMD and markedly higher expression of activated caspase-11 in eWAT of O-HFD (Figure 4C,D). These findings suggest that extracellular release of mature IL-1β is augmented in O-HFD by enhancement of activated caspase-11-mediated pore formation in eWAT.

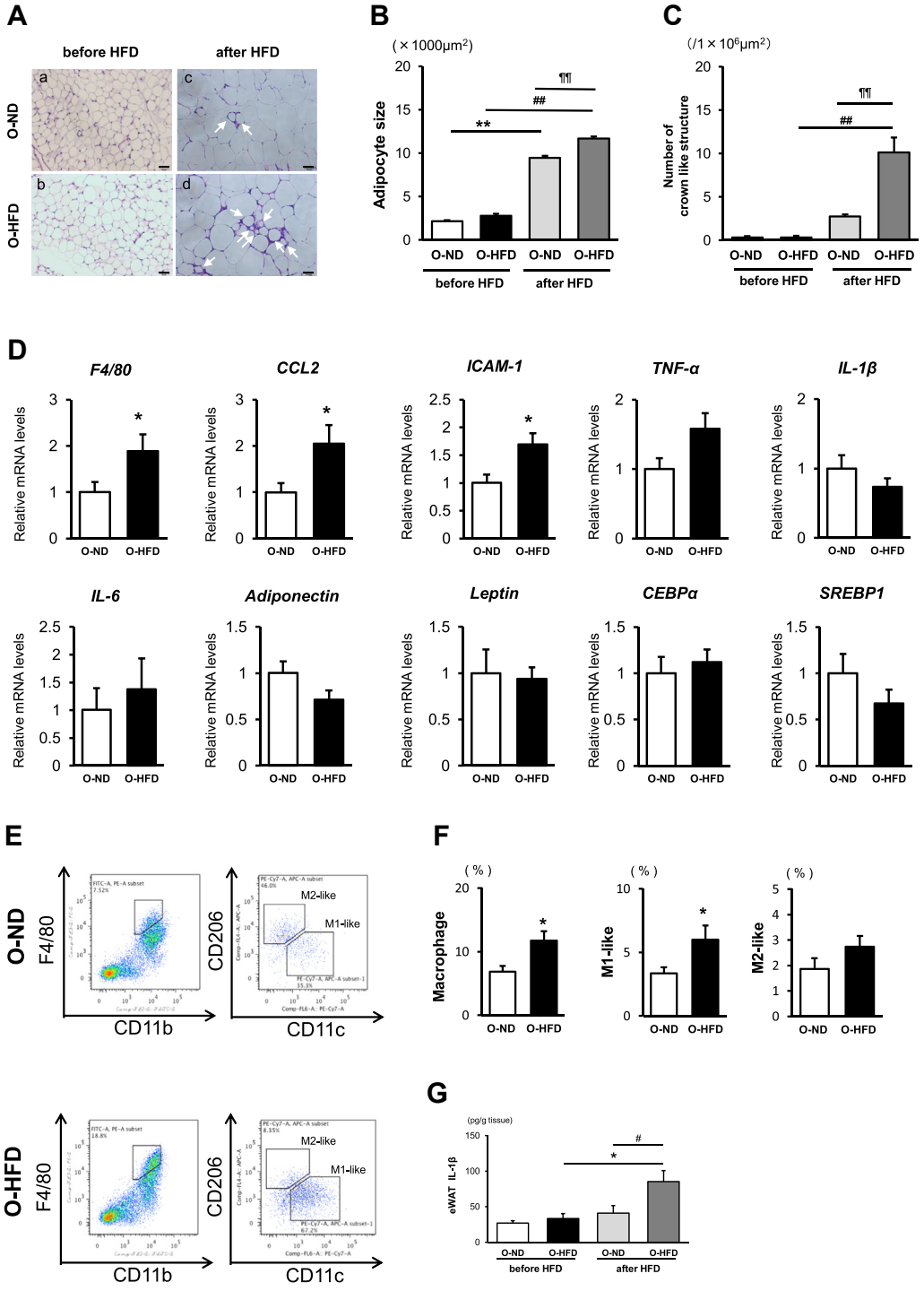

Figure 2: Maternal HFD enhances adipocyte size and the number of crown-like structures in eWAT. **(A)** Representative images of a hematoxylin-and-eosin-stained eWAT from O-ND (a, c) and O-HFD (b, d) mice before and after 8 weeks of HFD, respectively. The arrow shows CLS. Scale bar = 50 μm. O-ND, offspring of ND-fed dam; O-HFD, offspring of HFD-fed dam. (**B and C**) Quantitative analysis of adipocyte size and the number of CLSs. Values represent the mean ± SEM for 4 O-ND and 3 O-HFD mice before HFD, as well as 5 O-ND and 5 O-HFD mice after 8 weeks of HFD. $^{**}P < 0.01$ versus O-ND before HFD. $^{\#\#}P < 0.01$ versus O-HFD before HFD. $^{¶¶}P < 0.01$ versus O-ND after HFD. O-ND, offspring of ND-fed dam; O-HFD, offspring of HFD-fed dam. (**D**) Quantitative PCR analysis of mRNA expression levels in eWAT. Values represent the mean ± SEM relative to O-ND. Each group consisted of 6–9 O-ND and 8–9 O-HFD samples. $^{*}P < 0.05$ versus O-ND. O-ND, offspring of ND-fed dam; O-HFD, offspring of HFD-fed dam. (**E and F**) Flow cytometric analysis of F4/80, CD11b, CD206, and CD11c expressions in eWAT from O-ND and O-HFD mice after 8 weeks of HCD. Quantitative analysis shows a significant increase in macrophages and M1-like macrophages in O-HFD mice. Values are mean ± SEM for 7 O-ND and 6 O-HFD mice. $^{*}P < 0.05$ versus O-ND. O-ND, offspring of ND-fed dam; O-HFD, offspring of HFD-fed dam. (**G**) eWAT concentration of IL-1β after 8 weeks of HCD. Values are the mean ± SEM for 5 O-ND and 5 O-HFD mice before HFD, as well as 5 O-ND and 5 O-HFD mice after 8 weeks of HFD. $^{*}P < 0.05$ versus O-HFD before HFD. $^{\#}P < 0.05$ versus O-ND after HFD. O-ND, offspring of ND-fed dam; O-HFD, offspring of HFD-fed dam.

3.5. Membrane pore formation is augmented in BMDMs of offspring of HFD-fed dam

To further examine the augmented extracellular secretion of IL-1β via membrane pore formation, metabolic activation of BMDMs was performed by palmitate (PA) stimulation following lipopolysaccharide (LPS) priming [27]. After membrane pore formation, an increase in cytoplasmic osmolality results in the cell expansion and rupture, which are referred to as pyroptosis [39–42]. To examine the critical time points when the IL-1β release occurred in the living cells via membrane pore, we first performed LDH release assay. Consistent with the previously reported findings [37], LDH concentration in the supernatant was extremely low until 2-hour stimulation with PA in both two groups; however, it was markedly increased at 3 h after PA stimulation (Figure 5A). This finding suggests that membrane integrity was maintained within 2 h after PA stimulation. We then performed EtBr staining to examine pore formation without membrane destruction. Hoechst blue-stained macrophages show total cells in each field, and EtBr red-stained macrophages, as shown by the arrow, indicate permeabilized macrophages (Figure 5B). After PA stimulation following LPS priming, the percentage of EtBr-positive-staining cells is significantly increased in a time-dependent manner in both groups; however, their extent was significantly enhanced in O-HFD BMDMs (Figure 5C). This finding suggests that pore formation after metabolic stimulation was augmented in BMDMs of O-HFD.

3.6. Caspase-11 activity is enhanced in BMDMs of offspring of HFD-fed dam

Polarization to classically M1-like macrophage upon IFN-γ stimulation was almost equivalent between the two groups (Supplementary Figure 10A). Likewise, M2-like macrophage polarization upon IL-4 stimulation did not differ between the two groups (Supplementary Figure 10B). These findings are consistent with the finding that TNF-α concentration in the eWAT did not differ between O-ND and O-HFD. We next examined the noncanonical inflammasome activation pathway of caspase-11 in BMDMs upon metabolic activation. The expression level of procaspase-11 (p38) was significantly increased after LPS priming, which was much higher in O-HFD than that in O-ND (Figure 6A,B). Consistently, active caspase-11 (p26) was also significantly increased in BMDMs of O-HFD. In contrast, activation of caspase-1 by flow cytometric analysis did not show any difference between the two groups (Figure 6C,D). We further performed western blotting of caspase-1 in BMDMs. As shown in Figure 6E,F, the protein expression level of cleaved caspase-1, as well as procaspase-1, did not differ between the two groups before and after LPS priming, suggesting that the effect of LPS priming on procaspase-1 expression was compatible between the two groups. However, unexpectedly, the protein expression level of cleaved caspase-1 after metabolic activation tended to be higher in O-HFD than that in O-ND, although this did not reach statistical significance (Figure 6G,H). These results prompted us to examine whether the caspase-1 expression is indirectly enhanced by maternal HFD through the activation of caspase-11, because active caspase-11 in LPS-primed BMDMs has been shown to induce NLRP3 inflammasome activation by reducing intracellular potassium levels, resulting in the activation of caspase-1 [46].

3.7. Enhanced IL-1β release in BMDMs of offspring of HFD-fed dam is dependent on LPS priming

Finally, to examine the distinct relevance of the noncanonical inflammasome activation pathway of caspase-11 on extracellular IL-1β release, we analyzed supernatant IL-1β concentration with or without LPS priming because caspase-11 is activated by intracellular LPS but not PA (47–50). Without LPS priming, supernatant IL-1β concentration after PA stimulation was equivalent between the two groups. In contrast, with LPS priming, it was markedly increased in both groups of BMDMs; however, it was much higher in O-HFD than that in O-ND (Figure 7). These findings suggest that LPS priming plays a substantial role in the extravasation of mature IL-1β through membrane pore and supports the notion that noncanonical inflammasome activation pathway of caspase-11 by LPS priming primarily contributes to the augmented IL-1β release in BMDMs of O-HFD.

4. DISCUSSION

In this study, we showed for the first time that maternal high-fat diet increases the vulnerability to HFD-induced IR accompanied by augmented inflammasome activity in eWAT. Treatment with an inflammasome inhibitor completely abrogated HFD-induced IR in offspring of HFD-fed dam, suggesting that inflammasome activity plays a crucial role in enhancing HFD-induced IR resulting from maternal HFD feeding. Furthermore, *in vitro* IL-1β release from BMDMs upon stimulation with PA following LPS priming is significantly increased through the enhancement of GSDMD-mediated cell membrane pore formation via noncanonical inflammasome activation pathway of caspase-11, but not the canonical pathway of caspase-1. Our findings provide new insights into the causal association between maternal HFD and development of HFD-induced-IR in offspring, in which the noncanonical pathway of caspase-11 may contribute to HFD-evoked inflammasome activation in eWAT.

Inflammasome activation has been shown to play a crucial role in the development of HFD-induced IR through NLRP3-dependent activation of caspase-1, which cleaves pro-IL-1β into mature IL-1β [27–30]. However, previous studies have shown the contrary findings in the role of caspase-1 in HFD-induced obesity and insulin resistance [51,52]. Kimura H. et al. showed that caspase-1 deficiency promotes HFD-induced obesity and proinflammatory response in the adipose tissue [51], which was consistent with the findings by Wang et al. [52]. In contrast, Stienstra et al. demonstrated that caspase-1 deficiency eliminates HFD-induced BW gain [28]. We did not observe any difference in HFD-induced BW gain between O-ND and O-HFD, suggesting that active caspase-1 was less implicated in our experimental setting. On the other hand, CCL2 mRNA expression and subsequent accumulation of macrophages were significantly augmented in the eWAT of O-HFD compared with those of O-ND. Recently, Xu et al. investigated the role of GSDMD in the proinflammatory response using diet-induced nonalcoholic fatty liver disease model mice [53]. They showed that GSDMD was associated with the persistent activation of the NF-B signaling pathway and subsequent macrophage recruitment via CCL2 secretion. Furthermore, Unamuno et al. demonstrated that inhibition of NLRP3 in human visceral adipocytes significantly blocked LPS-induced upregulation of CCL2 [54]. Considering that protein expression levels of GSDMD and active caspase-11, which synergistically augment NLRP3 activation [55], were significantly enhanced in BMDMs from O-HFD, it is likely that enhanced accumulation of proinflammatory macrophages in the eWAT of O-HFD is attributed to the increased activation of caspase-11. Stienstra et al. also reported that caspase-1-deficient mice showed attenuated progression of HFD-induced IR, in which adipocytes are more contributable to caspase-1-mediated IL-1β secretion than macrophages in adipose tissue [56]. However, we examined caspase-1 activity in eWAT using ex vivo IVIS imaging and found that caspase-1 activity was equivalent between the offspring of ND-fed and HFD-fed dam, suggesting that caspase-1 activity in adipocytes, as well as macrophages, is not affected by

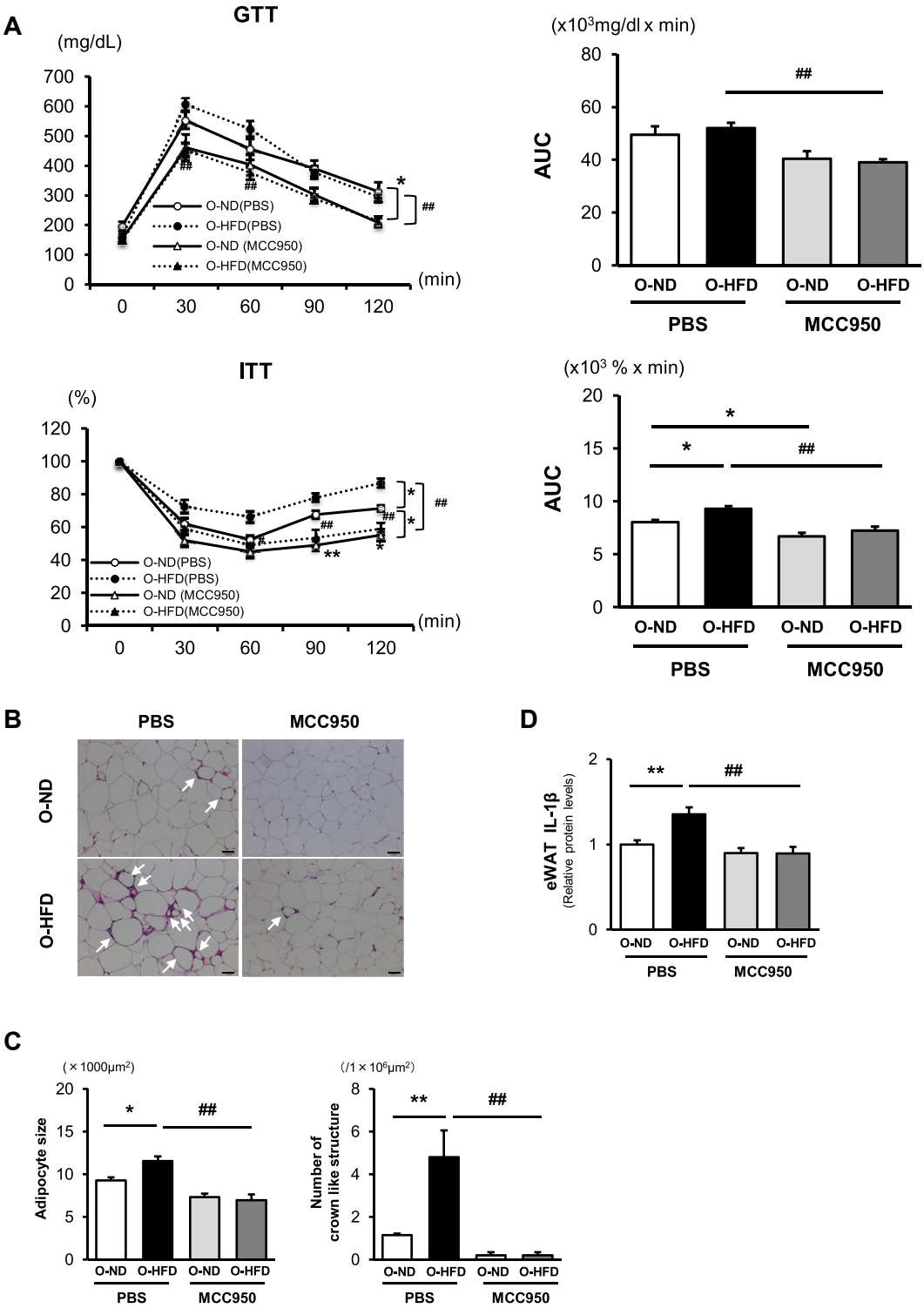

Figure 3: Inflammasome inhibitor treatment diminishes the accelerated insulin resistance development in O-HFD mice. (**A**) Glucose and insulin tolerance tests after 8 weeks of HFD. Values represent the mean ± SEM for 11 O-ND and 11 O-HFD mice treated with PBS, as well as 11 O-ND and 11 O-HFD mice treated with MCC950. $^{*}P < 0.05$ and $^{**}P < 0.01$ versus O-ND treated with PBS. $^{\#}P < 0.05$ and $^{\#\#}P < 0.01$ versus O-HFD treated with PBS. O-ND, offspring of ND-fed dam; O-HFD, offspring of HFD-fed dam; GTT, glucose tolerance test; ITT, insulin tolerance test, AUC, area under the curve. (**B**) Representative images of a hematoxylin-and-eosin-stained eWAT from O-ND and O-HFD mice, respectively. The arrow shows CLS. Scale bar = 50 μm. O-ND, offspring of ND-fed dam; O-HFD, offspring of HFD-fed dam. (**C**) Quantitative analysis of adipocyte size and the number of CLSs. Values represent the mean ± SEM. Each group consisted of five mice. $^{*}P < 0.05$ and $^{**}P < 0.01$ versus O-ND treated with PBS. $^{\#\#}P < 0.01$ versus O-HFD treated with PBS. O-ND, offspring of ND-fed dam; O-HFD, offspring of HFD-fed dam. (**D**) eWAT concentrations of IL-1β after 8 weeks of HCD with or without MCC950. Values are the mean ± SEM for 10 O-ND and 11 O-HFD mice treated with PBS, as well as 10 O-ND and 11 O-HFD mice treated with MCC950. Data were expressed as protein concentration levels relative to those of O-ND treated with PBS. $^{**}P < 0.01$ versus O-ND treated with PBS. $^{\#\#}P < 0.01$ versus O-HFD treated with PBS. O-ND, offspring of ND-fed dam; O-HFD, offspring of HFD-fed dam.

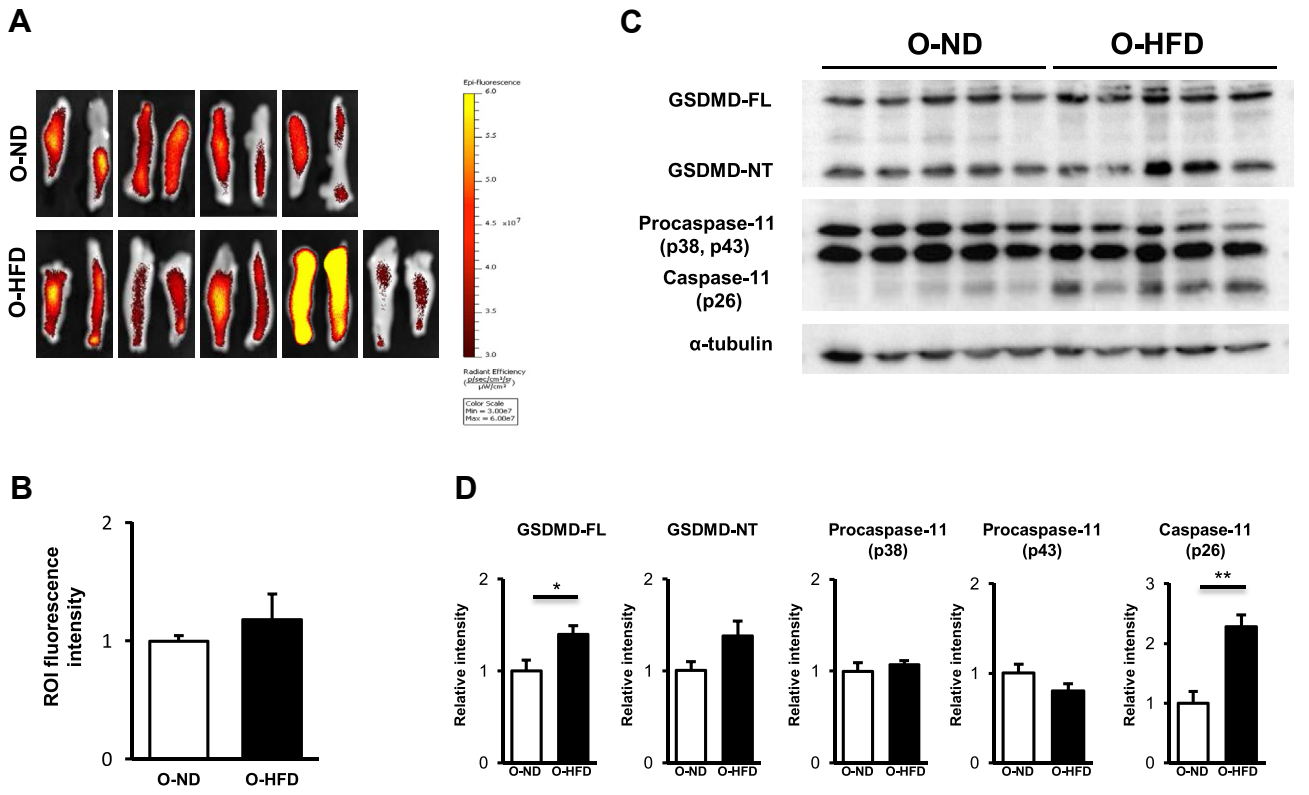

Figure 4: Noncanonical inflammasome activation pathway of caspase-11 is augmented in eWAT of O-HFD. (**A and B**) Representative ex vivo images of eWAT, as well as quantitative measurement of radiant efficiency corresponding to caspase-1 activity. Values are the mean ± SEM for 4 O-ND and 5 O-HFD mice. O-ND, offspring of ND-fed dam; O-HFD, offspring of HFD-fed dam. (**C and D**) Representative western blot of GSDMD and caspase-11 in eWAT, as well as quantitative analysis of protein expression. Values are the mean ± SEM for 5 O-ND and 5 O-HFD mice. $*P < 0.05$ and $**P < 0.01$ versus O-ND. O-ND, offspring of ND-fed dam; O-HFD, offspring of HFD-fed dam; GSDMD-FL, full length of gasdermin D; GSDMD-NT, N-terminal portion of gasdermin D.

maternal HFD. Kotas et al. reported that caspase-1-deficient mice showed a significant triglyceride clearance, which could affect HFD-induced IR development [57]. We also observed no difference in caspase-1 activity in liver, as well as serum FFA level, between the two groups of the offspring, suggesting that caspase-1-mediated modification of lipid metabolism is not likely to be responsible for the vulnerability to HFD-induced IR in the offspring of HFD-fed dam.

The noncanonical inflammasome activation pathway of caspase-11 has been intensively investigated and emerged as a potential therapeutic target of inflammatory diseases such as infectious diseases [58]. Although caspase-11, as well as caspase-1, cleaves GSDMD [44,45], caspase-11 itself does not have the ability to cleave proIL-1β and proIL-18. Therefore, the activation of NLRP3 is still needed for their maturation [38,39,44]. This is consistent with our finding that NLRP3-specific inhibitor completely abrogates HFD-induced IR in the offspring of HFD-fed dam despite the equivalent activity of caspase-1 between the two groups. NLRP3 inflammasome could be activated by various NLRP3 activators; however, the underlying mechanism has not been fully elucidated [59]. Perregaux et al. first reported that a reduction of intracellular potassium concentration is necessary for the activation of IL-1β upon ATP or nigericin stimulation in LPS-primed mouse peritoneal macrophages [60]. Recently, Muñoz-Planillo et al. showed that a loss of intracellular potassium is indispensable for NLRP3 activation in BMDMs [61]. Furthermore, Rühl et al. demonstrated that LPS-transfected BMDMs showed an increase in activity of caspase-11, which augmented potassium efflux, leading to NLRP3 inflammasome activation and subsequent IL-1β release [46]. Based on the results of these studies [62], we hypothesized that augmented pore formation via caspase-11-mediated cleavage of GSDMD could promote membrane permeabilization, leading to the reduction of intracellular potassium, thereby enhancing NLRP3 activation in O-HFD. We observed that the activation of caspase-11 was enhanced in O-HFD *in vivo* and *in vitro* experiments. Further, the percentage of membrane pore formation and subsequent IL-1β release into the culture supernatant were significantly increased in BMDMs of O-HFD upon PA stimulation following LPS priming. Recent studies have shown that caspase-11, but not caspase-1, is activated by directly binding to the intracellular LPS [47–50]. Consistently, enhanced IL-1β release was completely eliminated when BMDMs were activated by PA without LPS priming. Taken together, augmented IL-1β release in BMDMs of O-HFD is more likely to be attributed to the enhanced pore formation via caspase-11 activation upon LPS priming rather than the increased maturation of proIL-1β via caspase-1 activation.

Skeldon et al. recently reported that HFD-fed caspase-11-deficient mice (C57BL/6 strain) showed the equivalent BW gain and glucose tolerance compared to wild-type control mice [63]. However, the results of ITT and serum insulin levels were not presented in this experiment. The duration of HFD was much longer (16 weeks) in their experiment compared to our experiment (8 weeks). During the early stage of HFD-induced IR, glucose tolerance could be compensated by augmented insulin secretion [64,65]. Further, two caspase-12-deficient strains were investigated in their

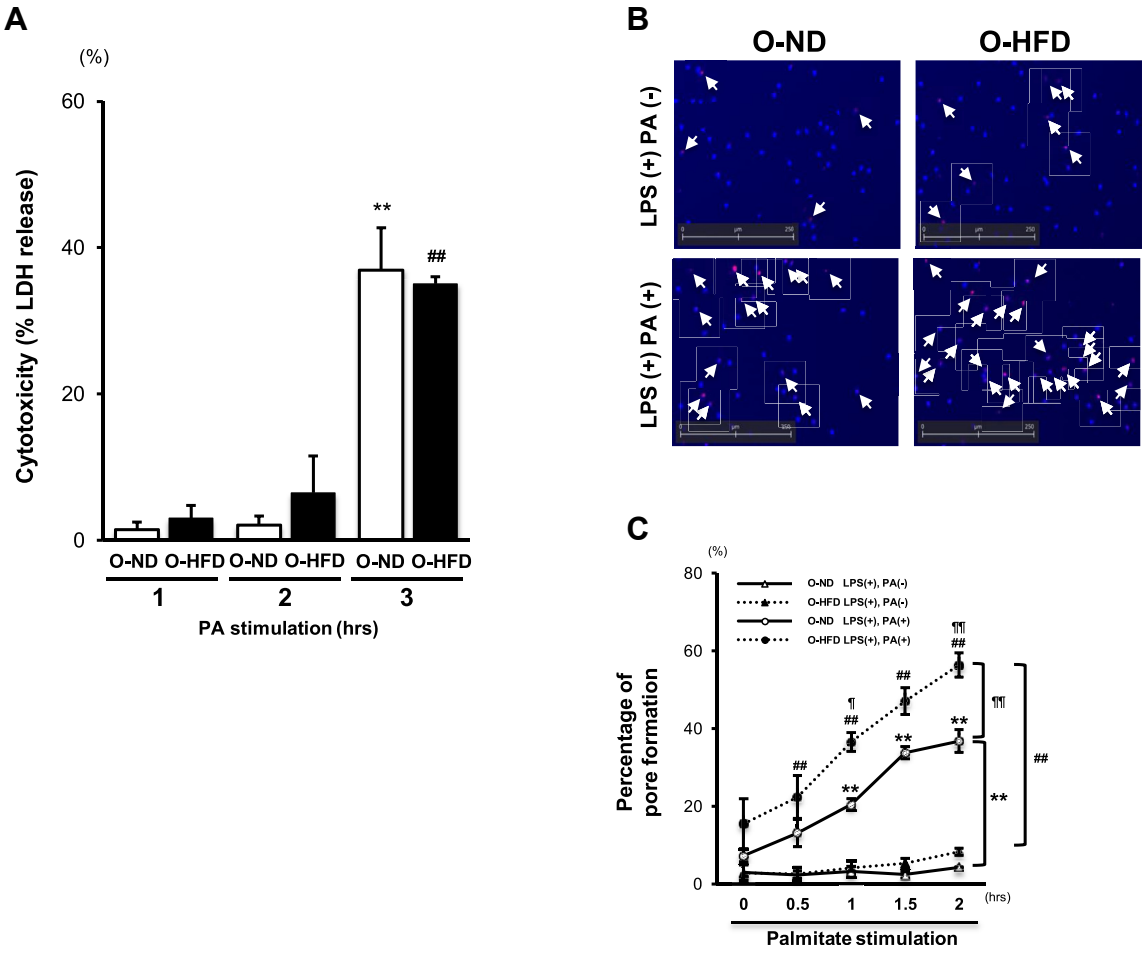

Figure 5: Membrane pore formation is augmented in BMDMs of O-HFD. (**A**) Lactate-dehydrogenase- (LDH-) release-based cell death in BMDMs after PA stimulation following LPS priming. Values are the mean ± SE for 5 O-ND and 5 O-HFD mice. $^{**}P < 0.01$ versus O-ND stimulated with PA (1 or 2 h). $^{\#\#}P < 0.01$ versus O-HFD stimulated with PA (1 or 2 h). LPS, lipopolysaccharide; PA, palmitate; O-ND, offspring of ND-fed dam; O-HFD, offspring of HFD-fed dam. (**B**) Representative images of pore formation in BMDMs 2 h after PA stimulation following LPS priming. Hoechst-stained BMDMs (blue) show total cells in each field, and EtBr (red) indicates permeabilized BMDMs. O-ND, offspring of ND-fed dam; O-HFD, offspring of HFD-fed dam. (**C**) Quantitative analysis of influx of EtBr after PA stimulation following LPS priming. Values are the mean ± SE for 3 O-ND and 3 O-HFD mice. $^{**}P < 0.01$ versus O-ND + LPS. $^{\#\#}P < 0.01$ versus O-HFD + LPS. $^{\P}P < 0.05$ versus O-ND + LPS + PA. $^{\P\P}P < 0.01$ versus O-ND + LPS + PA. O-ND, offspring of ND-fed dam; O-HFD, offspring of HFD-fed dam.

experiment: caspase-12-deficient mice (129 strain) that have a mutation in caspase-11- and caspase-12-deficient mice (C57BL/6 strain) that are sufficient for caspase-11. They observed a slight difference in adipose tissue phenotype after HFD between these two strains, suggesting that caspase-11 may contribute to the modulation of adipose tissue phenotype even during the late stage of HFD-induced IR. Likewise, caspase-1-deficient mice (129 strain) which have been widely investigated are containing a mutation in the caspase-11 locus that attenuates its expression [43]. It cannot be ruled out that caspase-11 may be involved in the development of HFD-induced IR observed in caspase-1-deficient mice. The relevant contribution of caspase-11 during the early stage of HFD-induced IR needs to be investigated using caspase-11-deficient mice (C57BL/6 strain) in future studies.

In contrast to caspase-1, intracellular LPS had initially been reported to be a sole activator of caspase-11 [47–50], which may explain why the role of caspase-11 in HFD-induced IR has been investigated less than its role in infection-mediated diseases caused by gram-negative bacteria. However, Cani et al. reported that a 4-week HFD chronically increased plasma LPS concentration [66]. Caesar et al. also showed the molecular mechanism of IR development through crosstalk between gut microbiota and adipose tissue inflammation via TRL signaling [67]. These findings raise the intriguing possibility that intracellular LPS, as well as extracellular LPS, elicits adipose tissue inflammation in the pathogenesis of HFD-induced IR. Recently, mechanistic insight into the activation of caspase-11 has been extensively investigated. Chu et al. demonstrated that intracellular oxidized phospholipid 1-palmitoyl-2-arachidonoyl-sn-glycero-3-phosphorylcholine (oxPAPC) prevents the direct binding of intracellular LPS to the CARD domain of caspase-11 in murine BMDMs [68]. oxPAPC has been reported to be present in the circulation and is increased during inflammation and infection [69]. Indeed, Serbulea et al. have recently shown that full-length oxPAPC increases in the stromal vascular fraction of eWAT in HFD-fed obese mice, which was significantly correlated with fat pad weight [70]. They also showed that full-length oxPAPC promotes inflammatory gene expression in BMDMs;

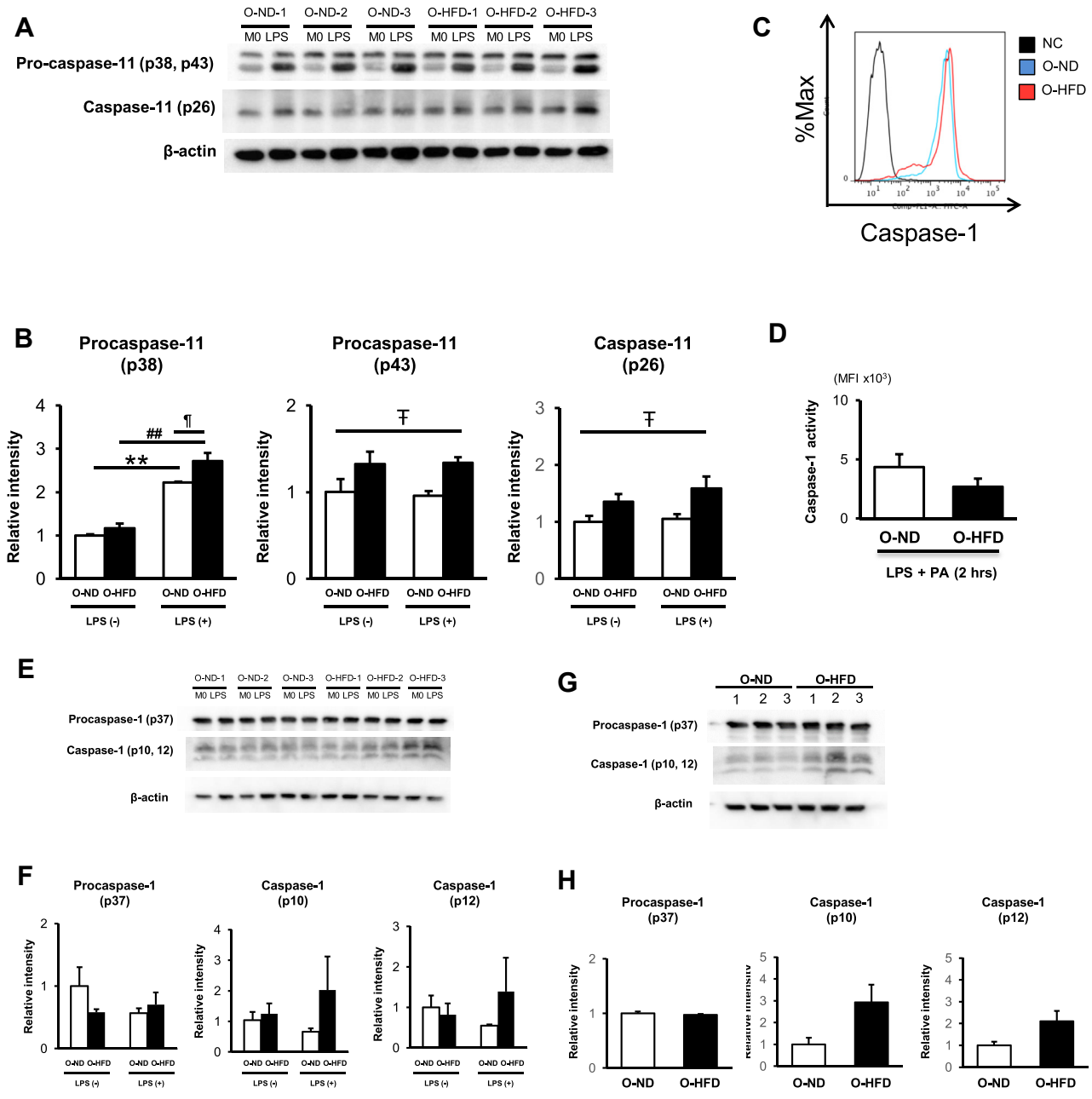

Figure 6: Caspase-11 activity is enhanced in BMDMs of O-HFD. (**A and B**) Representative western blot of caspase-11 of BMDMs before and after LPS priming as well as quantitative analysis of protein expressions. Values are the mean ± SE for 3 O-ND and 3 O-HFD mice before LPS priming, as well as 3 O-ND and 3 O-HFD mice after LPS priming. $^{**}P < 0.01$ versus O-ND (before LPS priming). $^{\#\#}P < 0.01$ versus O-HFD (before LPS priming). $^{\P}P < 0.05$ versus O-ND (after LPS priming). $^{\#}P < 0.05$ (O-ND versus O-HFD). LPS, lipopolysaccharide; M0, BMDMs before LPS priming; O-ND, offspring of ND-fed dam; O-HFD, offspring of HFD-fed dam. (**C and D**) Flow cytometric analysis of the caspase-1 activity in BMDMs, as well as quantitative analysis of MFI, after 2 h of PA stimulation following LPS priming. Values are the mean ± SEM for 5 O-ND and 5 O-HFD mice. LPS, lipopolysaccharide; PA, palmitate; O-ND, offspring of ND-fed dam; O-HFD, offspring of HFD-fed dam. (**E and F**) Representative western blot of caspase-1 of BMDMs before and after LPS priming as well as quantitative analysis of protein expressions. Values are the mean ± SE for 3 O-ND and 3 O-HFD mice before LPS priming, as well as 3 O-ND and 3 O-HFD mice after LPS priming. LPS, lipopolysaccharide; M0, BMDMs before LPS priming; O-ND, offspring of ND-fed dam; O-HFD, offspring of HFD-fed dam. (**G and H**) Representative western blot of caspase-1 of BMDMs after 2 h of PA stimulation following LPS priming as well as quantitative analysis of protein expressions. Values are the mean ± SE for 3 O-ND and 3 O-HFD mice. PA, palmitate; LPS, lipopolysaccharide; O-ND, offspring of ND-fed dam; O-HFD, offspring of HFD-fed dam.

however, given that fat pad weight and proinflammatory gene expression levels of eWAT were comparable between O-ND and O-HFD, it is not likely that oxPAPC is implicated in the enhanced activity of caspase-11 in the eWAT of O-HFD.

The maternal nutritional state has been demonstrated to be responsible for the dysfunctional metabolic homeostasis in adult offspring through epigenetic mechanisms, such as DNA methylation, post-translational modifications to histone proteins, and noncoding RNA without changing the underlying DNA sequence [12—15]. Numerous studies have shown that epigenetic mechanisms regulate NLRP3-mediated inflammasome via the canonical activation pathway of caspase-1 by increasing the production of inflammasome components

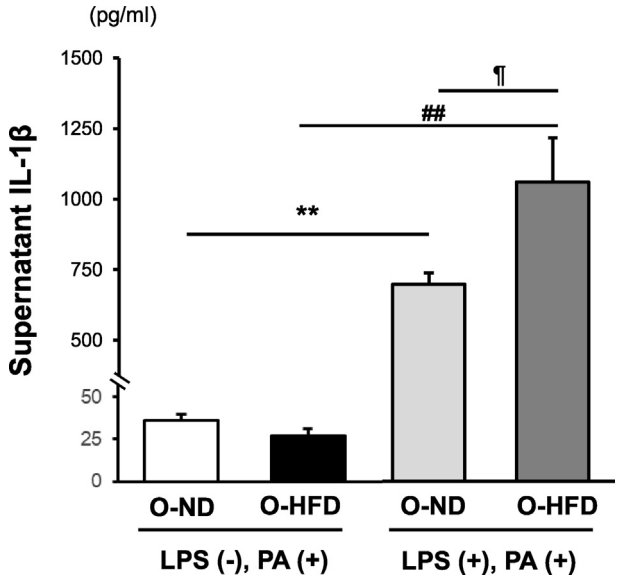

Figure 7: Mature IL-1β release is augmented in BMDMs of O-HFD after metabolic activation. Protein concentrations of IL-1β in the supernatant of BMDMs after metabolic activation. Values are the mean ± SE for 5 O-ND and 5 O-HFD mice without LPS priming, as well as 5 O-ND and 5 O-HFD mice with LPS priming. $^{**}P < 0.01$ versus O-ND (PA). $^{\#\#}P < 0.01$ versus O-HFD (PA). $^{\P}P < 0.05$ versus O-ND (LPS + PA). LPS, lipopolysaccharide; PA, palmitate; O-ND, offspring of ND-fed dam; O-HFD, offspring of HFD-fed dam.

[71,72]; however, studies investigating epigenetic regulation of non-canonical activation pathway of caspase-11 are sparse and need to be elucidated in future studies.

5. CONCLUSION

Our study demonstrates that maternal HFD exhibits inflammasome activation in eWAT of offspring and subsequently accelerates HFD-induced IR. Furthermore, *in vitro* caspase-11 activation of BMDMs of offspring of HFD-fed dam was significantly augmented and accompanied by the increased membrane pore formation and subsequent release of IL-1β. These findings support the notion that caspase-11 activation plays a critical role in maternal HFD-mediated HFD-induced IR development in offspring and sheds new insights into the underlying mechanism of maternal HFD-related CVD development by focusing on the modulation of macrophage function.

FUNDING

This paper has no funding.

AUTHORS' CONTRIBUTIONS

Contributions of each author are as follows: study design, N.W. and H.Y.; experiment conduction, N.W., H.Y., S.M., K.Y., S.M., H.K., D.M.; data analysis, N.W. and H.Y.; manuscript preparation, N.W. and H.Y.; study discussion and revision of the manuscript, N.W., H. Y., N. W., D.K., T.O., and S.M.

ACKNOWLEDGMENTS

This study was supported by JSPS KAKENHI (Grant number JP15K09162).

CONFLICT OF INTEREST

None declared.

APPENDIX A. SUPPLEMENTARY DATA

Supplementary data to this article can be found online at https://doi.org/10.1016/j.molmet.2020.100988.

REFERENCES

[1] The GBD 2013 Obesity Collaboration, 2014. Global, regional, and national prevalence of overweight and obesity in children and adults during 1980–2013: a systematic analysis for the Global Burden of Disease Study 2013. Lancet 384:766–781.

[2] NCD Risk Factor Collaboration (NCD-RisC), 2017. Worldwide trends in body-mass index, underweight, overweight, and obesity from 1975 to 2016: a pooled analysis of 2416 population-based measurement studies in 128·9 million children, adolescents, and adults. Lancet 390:2627–2642.

[3] Bornfeldt, K.E., Tabas, I., 2011. Insulin resistance, hyperglycemia, and atherosclerosis. Cell Metabolism 14:575–585.

[4] Laakso, M., Kuusisto, J., 2014. Insulin resistance and hyperglycaemia in cardiovascular disease development. Nature Review Endocrinology 10:293–302.

[5] Ormazabal, V., Nair, S., Elfeky, O., Aguayo, C., Salomon, C., Zuñiga, F.A., 2018. Association between insulin resistance and the development of cardiovascular disease. Cardiovascular Diabetology 17:122.

[6] Twig, G., Yaniv, G., Levine, H., Leiba, A., Goldberger, N., Derazne, E., et al., 2016. Body-Mass index in 2.3 million adolescents and cardiovascular death in adulthood. The New England Journal of Medicine 374:2430–2440.

[7] Drake, A.J., Reynolds, R.M., 2010. Impact of maternal obesity on offspring obesity and cardiometabolic disease risk. Reproduction 140:387–398.

[8] Hochner, H., Friedlander, Y., Calderon-Margalit, R., Meiner, V., Sagy, Y., Avgil-Tsadok, M., et al., 2012. Associations of maternal prepregnancy body mass index and gestational weight gain with adult offspring cardiometabolic risk factors: the Jerusalem Perinatal Family Follow-up Study. Circulation 125:1381–1389.

[9] Yu, Z., Han, S., Zhu, J., Sun, X., Ji, C., Guo, X., 2013. Pre-pregnancy body mass index in relation to infant birth weight and offspring overweight/obesity: a systematic review and meta-analysis. PloS One 8:e61627.

[10] Reynolds, R.M., Allan, K.M., Raja, E.A., Bhattacharya, S., McNeill, G., Hannaford, P.C., et al., 2013. Maternal obesity during pregnancy and premature mortality from cardiovascular event in adult offspring: follow-up of 1 323 275 person years. British Medical Journal 347:f4539.

[11] Gaillard, R., Steegers, E.A., Duijts, L., Felix, J.F., Hofman, A., Franco, O.H., et al., 2014. Childhood cardiometabolic outcomes of maternal obesity during pregnancy: the Generation R Study. Hypertension 63:683–691.

[12] Napoli, C., Infante, T., Casamassimi, A., 2011. Maternal-foetal epigenetic interactions in the beginning of cardiovascular damage. Cardiovascular Research 92:367–374.

[13] Napoli, C., Crudele, V., Soricelli, A., Al-Omran, M., Vitale, N., Infante, T., et al., 2012. Primary prevention of atherosclerosis: a clinical challenge for the reversal of epigenetic mechanisms? Circulation 125:2363–2373.

[14] Geraghty, A.A., Lindsay, K.L., Alberdi, G., McAuliffe, F.M., Gibney, E.R., 2016. Nutrition during pregnancy impacts offspring's epigenetic status-evidence from human and animal studies. Nutrition and Metabolic Insights 8:41–47.

[15] Lecoutre, S., Petrus, P., Rydén, M., Breton, C., 2018. Transgenerational epigenetic mechanisms in adipose tissue development. Trends Endocrinology Metabolism 29:675–685.

[16] Muhlhausler, B.S., Duffield, J.A., McMillen, I.C., 2007. Increased maternal nutrition stimulates peroxisome proliferator activated receptor-gamma,

adiponectin, and leptin messenger ribonucleic acid expression in adipose tissue before birth. Endocrinology 148:878–885.
[17] Elahi, M.M., Cagampang, F.R., Mukhtar, D., Anthony, F.W., Ohri, S.K., Hanson, M.A., 2009. Long-term maternal high-fat feeding from weaning through pregnancy and lactation predisposes offspring to hypertension, raised plasma lipids and fatty liver in mice. British Journal of Nutrition 102:514–519.
[18] Masuyama, H., Hiramatsu, Y., 2012. Effects of a high-fat diet exposure in utero on the metabolic syndrome-like phenomenon in mouse offspring through epigenetic changes in adipocytokine gene expression. Endocrinology 153:2823–2830.
[19] Borengasser, S.J., Zhong, Y., Kang, P., Lindsey, F., Ronis, M.J., Badger, T.M., et al., 2013. Maternal obesity enhances white adipose tissue differentiation and alters genome-scale DNA methylation in male rat offspring. Endocrinology 154:4113–4125.
[20] Wakana, N., Irie, D., Kikai, M., Terada, K., Yamamoto, K., Kawahito, H., et al., 2015. Maternal high-fat diet exaggerates atherosclerosis in adult offspring by augmenting periaortic adipose tissue-specific proinflammatory response. Arteriosclerosis, Thrombosis, and Vascular Biology 35:558–569.
[21] Lumeng, C.N., Bodzin, J.L., Saltiel, A.R., 2007. Obesity induces a phenotypic switch in adipose tissue macrophage polarization. Journal of Clinical Investigation 117:175–184.
[22] Coats, B.R., Schoenfelt, K.Q., Barbosa-Lorenzi, V.C., Peris, E., Cui, C., Hoffman, A., et al., 2017. Metabolically activated adipose tissue macrophages perform detrimental and beneficial functions during diet-induced obesity. Cell Reports 20:3149–3161.
[23] Russo, L., Lumeng, C.N., 2018. Properties and functions of adipose tissue macrophages in obesity. Immunology 155:407–417.
[24] Guilherme, A., Virbasius, J.V., Puri, V., Czech, M.P., 2008. Adipocyte dysfunctions linking obesity to insulin resistance and type 2 diabetes. Nature Reviews Molecular Cell Biology 9:367–377.
[25] Odegaard, J.I., Chawla, A., 2013. Pleiotropic actions of insulin resistance and inflammation in metabolic homeostasis. Science 339:172–177.
[26] Tchernof, A., Després, J.P., 2013. Pathophysiology of human visceral obesity: an update. Physiological Reviews 93:359–404.
[27] Wen, H., Gris, D., Lei, Y., Jha, S., Zhang, L., Huang, M.T., et al., 2011. Fatty acid-induced NLRP3-ASC inflammasome activation interferes with insulin signaling. Nature Immunology 12:408–415.
[28] Stienstra, R., van Diepen, J.A., Tack, C.J., Zaki, M.H., van de Veerdonk, F.L., Perera, D., et al., 2011. Inflammasome is a central player in the induction of obesity and insulin resistance. Proceedings of the National Academy of Sciences 108:15324–15329.
[29] Vandanmagsar, B., Youm, Y.H., Ravussin, A., Galgani, J.E., Stadler, K., Mynatt, R.L., et al., 2011. The NLRP3 inflammasome instigates obesity-induced inflammation and insulin resistance. Nature Medicine 17:179–188.
[30] Rheinheimer, J., de Souza, B.M., Cardoso, N.S., Bauer, A.C., Crispim, D., 2017. Current role of the NLRP3 inflammasome on obesity and insulin resistance: a systematic review. Metabolism 74:1–9.
[31] van der Heijden, T., Kritikou, E., Venema, W., van Duijn, J., van Santbrink, P.J., Slütter, B., et al., 2017. NLRP3 inflammasome inhibition by MCC950 reduces atherosclerotic lesion development in apolipoprotein E-deficient mice-brief report. Arteriosclerosis, Thrombosis, and Vascular Biology 37:1457–1461.
[32] Tsubakimoto, Y., Yamada, H., Yokoi, H., Kishida, S., Takata, H., Kawahito, H., et al., 2009. Bone marrow angiotensin AT1 receptor regulates differentiation of monocyte lineage progenitors from hematopoietic stem cells. Arteriosclerosis, Thrombosis, and Vascular Biology 29:1529–1536.
[33] Swirski, F.K., Libby, P., Aikawa, E., Alcaide, P., Luscinskas, F.W., Weissleder, R., et al., 2007. Ly-6Chi monocytes dominate hypercholesterolemia-associated monocytosis and give rise to macrophages in atheromata. Journal of Clinical Investigation 117:195–205.
[34] Cho, K.W., Morris, D.L., Lumeng, C.N., 2014. Flow cytometry analyses of adipose tissue macrophages. Methods in Enzymology 537:297–314.
[35] Sakhon, O.S., Victor, K.A., Choy, A., Tsuchiya, T., Eulgem, T., Pedra, J.H., 2013. NSD1 mitigates caspase-1 activation by listeriolysin O in macrophages. PloS One 8:e75911.
[36] Khallou-Laschet, J., Varthaman, A., Fornasa, G., Compain, C., Gaston, A.T., Clement, M., et al., 2010. Macrophage plasticity in experimental atherosclerosis. PloS One 5:e8852.
[37] Silveira, T.N., Zamboni, D.S., 2010. Pore formation triggered by Legionella spp. is an Nlrc4 inflammasome-dependent host cell response that precedes pyroptosis. Infection and Immunity 78:1403–1413.
[38] Van Opdenbosch, N., Lamkanfi, M., 2019. Caspases in cell death, inflammation, and disease. Immunity 50:1352–1364.
[39] Shi, J., Zhao, Y., Wang, K., Shi, X., Wang, Y., Huang, H., et al., 2015. Cleavage of GSDMD by inflammatory caspases determines pyroptotic cell death. Nature 526:660–665.
[40] Liu, X., Zhang, Z., Ruan, J., Pan, Y., Magupalli, V.G., Wu, H., et al., 2016. Inflammasome-activated gasdermin D causes pyroptosis by forming membrane pores. Nature 535:153–158.
[41] Sborgi, L., Rühl, S., Mulvihill, E., Pipercevic, J., Heilig, R., Stahlberg, H., et al., 2016. GSDMD membrane pore formation constitutes the mechanism of pyroptotic cell death. The EMBO Journal 35:1766–1778.
[42] Evavold, C.L., Ruan, J., Tan, Y., Xia, S., Wu, H., Kagan, J.C., 2018. The pore-forming protein gasdermin D regulates interleukin-1 secretion from living macrophages. Immunity 48:35–44 e6.
[43] Kayagaki, N., Warming, S., Lamkanfi, M., Vande Walle, L., Louie, S., Dong, J., et al., 2011. Non-canonical inflammasome activation targets caspase-11. Nature 479:117–121.
[44] Kayagaki, N., Stowe, I.B., Lee, B.L., O'Rourke, K., Anderson, K., Warming, S., et al., 2015. Caspase-11 cleaves gasdermin D for non-canonical inflammasome signalling. Nature 526:666–671.
[45] Aglietti, R.A., Estevez, A., Gupta, A., Ramirez, M.G., Liu, P.S., Kayagaki, N., et al., 2016. GsdmD p30 elicited by caspase-11 during pyroptosis forms pores in membranes. Proceedings of the National Academy of Sciences 113:7858–7863.
[46] Rühl, S., Broz, P., 2015. Caspase-11 activates a canonical NLRP3 inflammasome by promoting K(+) efflux. European Journal of Immunology 45:2927–2936.
[47] Kayagaki, N., Wong, M.T., Stowe, I.B., Ramani, S.R., Gonzalez, L.C., Akashi-Takamura, S., et al., 2013. Noncanonical inflammasome activation by intracellular LPS independent of TLR4. Science 341:1246–1249.
[48] Shi, J., Zhao, Y., Wang, Y., Gao, W., Ding, J., Li, P., et al., 2014. Inflammatory caspases are innate immune receptors for intracellular LPS. Nature 514:187–192.
[49] Yi, Y.S., 2017. Caspase-11 non-canonical inflammasome: a critical sensor of intracellular lipopolysaccharide in macrophage-mediated inflammatory responses. Immunology 152:207–217.
[50] Lee, B.L., Stowe, I.B., Gupta, A., Kornfeld, O.S., Roose-Girma, M., Anderson, K., et al., 2018. Caspase-11 auto-proteolysis is crucial for noncanonical inflammasome activation. Journal of Experimental Medicine 215:2279–2288.
[51] Kimura, H., Karasawa, T., Usui, F., Kawashima, A., Endo, Y., Kobayashi, M., et al., 2016 Nov 1. Caspase-1 deficiency promotes high-fat diet-induced adipose tissue inflammation and the development of obesity. American Journal of Physiology Endocrinology and Metabolism 311(5):E881–E890.
[52] Wang, H., Capell, W., Yoon, J.H., Faubel, S., Eckel, R.H., 2014. Obesity development in caspase-1-deficient mice. International Journal of Obesity (Lond) 38:152–155.
[53] Xu, B., Jiang, M., Chu, Y., Wang, W., Chen, D., Li, X., 2018. Gasdermin D plays a key role as a pyroptosis executor of non-alcoholic steatohepatitis in humans and mice. Journal of Hepatology 68:773–782.
[54] Unamuno, X., Gómez-Ambrosi, J., Ramírez, B., Rodríguez, A., Becerril, S., Valentí, V., 2019 Sep 24. NLRP3 inflammasome blockade reduces adipose

tissue inflammation and extracellular matrix remodeling. Cellular and Molecular Immunology [Epub ahead of print].

[55] Swanson, K.V., Deng, M., Ting, J.P., 2019. The NLRP3 inflammasome: molecular activation and regulation to therapeutics. Nature Review Immunology 19:477—489.

[56] Stienstra, R., Joosten, L.A., Koenen, T., van Tits, B., van Diepen, J.A., van den Berg, S.A., et al., 2010. The inflammasome-mediated caspase-1 activation controls adipocyte differentiation and insulin sensitivity. Cell Metabolism 12:593—605.

[57] Kotas, M.E., Jurczak, M.J., Annicelli, C., Gillum, M.P., Cline, G.W., Shulman, G.I., et al., 2013. Role of caspase-1 in regulation of triglyceride metabolism. Proceedings of the National Academy of Sciences 110:4810—4815.

[58] Yi, Y.S., 2018. Regulatory roles of the caspase-11 non-canonical inflammasome in inflammatory diseases. Immune Network 18:e41.

[59] Mishra, P.K., Adameova, A., Hill, J.A., Baines, C.P., Kang, P.M., Downey, J.M., et al., 2019. Guidelines for evaluating myocardial cell death. American Journal of Physiology - Heart and Circulatory Physiology 317:H891—H922.

[60] Perregaux, D., Gabel, C.A., 1994. Interleukin-1 beta maturation and release in response to ATP and nigericin. Evidence that potassium depletion mediated by these agents is a necessary and common feature of their activity. Journal of Biological Chemistry 269:15195—15203.

[61] Muñoz-Planillo, R., Kuffa, P., Martínez-Colón, G., Smith, B.L., Rajendiran, T.M., Núñez, G., 2013. K^+ efflux is the common trigger of NLRP3 inflammasome activation by bacterial toxins and particulate matter. Immunity 38:1142—1153.

[62] Yi, Y.S., 2020. Functional crosstalk between non-canonical caspase-11 and canonical NLRP3 inflammasomes during infection-mediated inflammation. Immunology 159:142—155.

[63] Skeldon, A.M., Morizot, A., Douglas, T., Santoro, N., Kursawe, R., Kozlitina, J., et al., 2016. Caspase-12, but not caspase-11, inhibits obesity and insulin resistance. The Journal of Immunology 196:437—447.

[64] Kasuga, M., 2006. Insulin resistance and pancreatic β cell failure. Journal of Clinical Investigation 116:1756—1760.

[65] Czech, M.P., 2017. Insulin action and resistance in obesity and type 2 diabetes. Nature Medicine 23:804—814.

[66] Cani, P.D., Amar, J., Iglesias, M.A., Poggi, M., Knauf, C., Bastelica, D., et al., 2007. Metabolic endotoxemia initiates obesity and insulin resistance. Diabetes 56:1761—1772.

[67] Caesar, R., Tremaroli, V., Kovatcheva-Datchary, P., Cani, P.D., Bäckhed, F., 2015. Crosstalk between gut microbiota and dietary lipids aggravates WAT inflammation through TLR signaling. Cell Metabolism 22:658—668.

[68] Chu, L.H., Indramohan, M., Ratsimandresey, R.A., Gangopadhyay, A., Morris, E.P., Monack, D.M., et al., 2018. The oxidized phospholipid oxPAPC protects from septic shock by targeting the non-canonical inflammasome in macrophages. Nature Communications 9:996.

[69] Frey, B., Haupt, R., Alms, S., Holzmann, G., König, T., Kern, H., et al., 2000. Increase in fragmented phosphatidylcholine in blood plasma by oxidative stress. The Journal of Lipid Research 41:1145—1153.

[70] Serbulea, V., Upchurch, C.M., Schappe, M.S., Voigt, P., DeWeese, D.E., Desai, B.N., et al., 2018. Macrophage phenotype and bioenergetics are controlled by oxidized phospholipids identified in lean and obese adipose tissue. Proceedings of the National Academy of Sciences 115:E6254—E6263.

[71] Neudecker, V., Haneklaus, M., Jensen, O., Khailova, L., Masterson, J.C., Tye, H., et al., 2017. Myeloid-derived miR-223 regulates intestinal inflammation via repression of the NLRP3 inflammasome. Journal of Experimental Medicine 214:1737—1752.

[72] Surace, A.E.A., Hedrich, C.M., 2019. The role of epigenetics in autoimmune/inflammatory disease. Frontiers in Immunology 10:1525.

